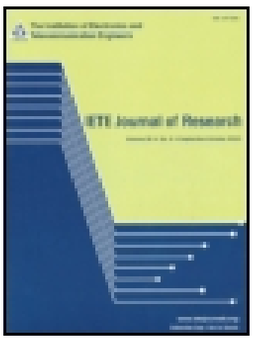

IETE Journal of Research

ISSN: 0377-2063 (Print) 0974-780X (Online) Journal homepage: https://www.tandfonline.com/loi/tijr20

An Automated Algorithm to Extract Time Plane Features From the PPG Signal and its Derivatives for Personal Health Monitoring Application

Abhishek Chakraborty, Deboleena Sadhukhan & Madhuchhanda Mitra

To cite this article: Abhishek Chakraborty, Deboleena Sadhukhan & Madhuchhanda Mitra (2019): An Automated Algorithm to Extract Time Plane Features From the PPG Signal and its Derivatives for Personal Health Monitoring Application, IETE Journal of Research, DOI: 10.1080/03772063.2019.1604178

To link to this article: https://doi.org/10.1080/03772063.2019.1604178

Published online: 16 Apr 2019.

IETE JOURNAL OF RESEARCH
https://doi.org/10.1080/03772063.2019.1604178

An Automated Algorithm to Extract Time Plane Features From the PPG Signal and its Derivatives for Personal Health Monitoring Application

Abhishek Chakraborty, Deboleena Sadhukhan and Madhuchhanda Mitra

Department of Applied Physics, University of Calcutta, Kolkata, West Bengal, India

ABSTRACT

Recently, photoplethysmogram (PPG) signal is widely adopted in health monitoring devices for automated assessment of different cardiovascular parameters. However, research in the area of computerized health analysis using PPG signal features is still lagging behind. In this paper, a robust, automated yet simple algorithm is proposed for accurate detection of characteristic points from the PPG signal and its derivatives. The methodology follows amplitude thresholding, slope-reversal, and an empirical formula based approach. Finally, Baseline modulation is removed from the PPG dataset and features are extracted from the amplitude normalized PPG signal and its derivatives. Performance of the proposed algorithm is evaluated over MIMIC database as well as over real PPG data acquired from both healthy volunteers and cardiac patients. The algorithm exhibits high efficiency for all detected fiducial points with an average sensitivity, positive predictivity and detection accuracy of 99.80%, 99.84%, and 99.65%, respectively. Compared to the existing methods, the proposed algorithm offers complete characterization of the PPG signal and its derivatives.

KEYWORDS

Amplitude threshold; Biomedical signal processing; Photoplethysmogram (PPG); PPG derivatives; Slope reversal; Time-domain feature extraction

1. INTRODUCTION

Over the past decades rapid changes in lifestyle, food habits, and increasing stress levels have led to the outbreak of different chronic cardiovascular diseases (CVDs) among the population [1]. Although, till date the medical assistance needed to deal with post-cardiovascular complications at the public sector healthcare facilities, especially in the rural areas are found to be vastly inadequate due to the lack of infrastructure and less availability of trained medical personnel [2]. Consequently, the importance of pre-diagnosis, obtained from regular monitoring of vital signs has been increasing day by day around the world as a life saving and cost-effective alternative. Towards this purpose, experts are now trying to bring healthcare facilities at home in the form of a low cost, battery operated, portable health monitoring devices [3]. However, such hand held devices are adaptable only with reliable and easy biosignal acquisition technology, which allows full patient comfort. Hence, photoplethysmogram (PPG) is widely accepted in such clinical establishments as a promising alternative of existing standard bio-signals. Moreover, PPG acquisition set up doesn't involve the requirement of any gel, external stimulus, electrodes or an expert operator as needed for other bio-signals [4,5].

Photoplethysmogram (PPG) signal is used to detect relative blood volume changes in the peripheral body sites (*i.e.* finger tip, earlobe, and toe). Contemporary PPG acquisition module uses a light emitting diodes (LED) to illuminate the tissues and a photodiode to measure the amount of reflected or transmitted light [5]. Inherently, PPG signal consist of a pulsatile ac component (signifies average blood volume change) superimposed on a quasi-dc component (representing respiration and sympathetic nervous activity *etc.*), as shown in Figure 1(a). The onset of each pulse indicates the commencement of blood ejection from the heart to the aorta. The end of ejection is manifested in the form of dicrotic notch, indicating closure of the aortic valve [5].

Primarily, PPG signal features were used in the measurement of blood oxygen saturation level (SpO2) [6]. However, due to associated easy acquisition technology, PPG signal has now been extensively used in various researches as a surrogate of other bio-signals. Morphological resemblance between PPG and blood pressure (ABP) waveforms have motivated the researchers to develop different cuff-less blood pressure estimation models, based on PPG signal features [7]. Moreover, apart from heart rate [8], respiration [9], emotion recognition [10], sleep apnea detection [11], PPG signal features has been widely used as a substitute of ECG, to assess different cardiovascular diseases like myocardial infarction [12], atrial fibrillation [13] and premature ventricular contractions [14]. However, factors like

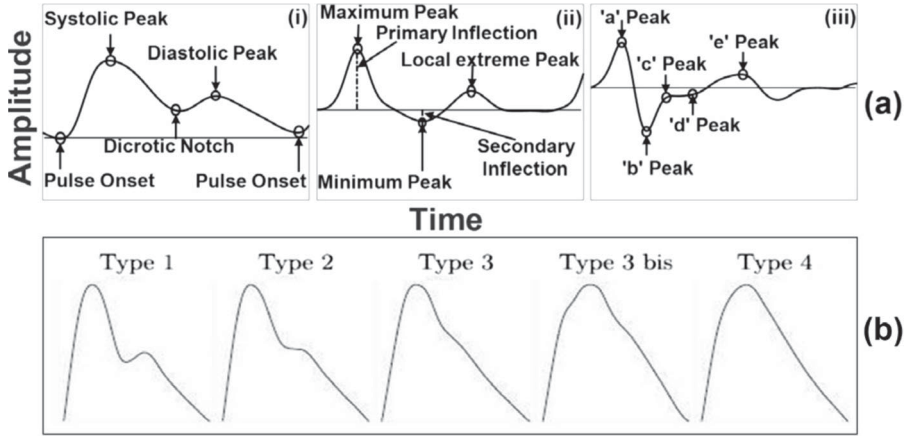

Figure 1: (a) Illustrative description of the (i) PPG, (ii) FDPPG and (iii) SDPPG signals with all characteristic points. (b) Different types of PPG signal [13].

amount of pressure variation on the sensor tip during data acquisition, the presence of motion artifact, noisy ambient, position of the sensor with respect to the heart might affect the performance of any PPG signal based measurement [15].

In addition, considering high sensitivity of the PPG signal morphology to age, gender and pathophysiological changes [5], different types of PPG signal morphologies are shown in Figure 1(b). From Figure 1(b), it is clear that, except for Type-1 and Type-2, the location of dicrotic notch is not prominent in any other types. In such cases, effective signal enhancement and quantification can be done by analyzing first (FDPPG) and second derivative (SDPPG) of the PPG signals with minimal computational complexity. Usually, FDPPG wave consist of a maximum peak, a minimum peak and a local extreme point, whereas in general four systolic waves ("*a*", "*b*", "*c*" and "*d*" waves) and one diastolic wave ("*e*" wave) related to the dicrotic notch are found to be associated with the SDPPG waveform as illustrated in Figure 1(a) [16].

So far, few dedicated algorithms have been proposed in the literatures for the detection of fiducial points from the PPG signal or its derivatives (mostly SDPPG) [17–27]. These methods can be broadly categorized into three types: (1) transform based techniques [17–18], (2) morphological analysis of the PPG signal derivative [19–24], and (3) morphological analysis of the PPG signal itself [25–27]. In [17] and [18], a Hilbert transform and wavelet transform (SWT) based algorithm is proposed to identify systolic peak and pulse onset points. However, instead of good performance, complicated mathematical steps associated in the transformation based techniques makes the signal analysis more computationally intensive for implementation in an embedded platform. In [19–24] the proposed algorithms uses derivative based methods to identify fiducial points from the PPG signal or its derivatives. Usually, signal analysis based on derivative methods is noise sensitive. This calls for pre-filtering of the signal as an essential step for further analysis. Signal morphology-based analysis is carried out in [25–27] to identify fiducial points like pulse onset, systolic peak [25], [26] or dicrotic notch [27]. In such cases, low-frequency nature and variance of signal morphology under pathophysiological variation often causes obscurity of fiducial points which imposes serious limitations for signal analysis. As a whole, most of the above-mentioned algorithms are lagging behind due to either: (1) partial characterization of the PPG signal or its derivatives or (2) use of a database containing PPG signals with much less or no pathophysiological variety. To the best knowledge of the authors of this article, no literature has been proposed till date focusing on complete characterization of the PPG signal and its derivatives with accurate feature extraction. Hence, in this research, a robust, automated yet simple algorithm is proposed to meet the requirements of portable health monitoring systems with limited computational resources. The proposed algorithm is designed to detect all the necessary fiducial points with simultaneous extraction of clinically important features from the PPG signal and its derivatives. The database used by the algorithm contains both healthy and pathological data with significant morphological and pathological variations. The rest of this paper is presented as follows. Methodology of the proposed algorithm is presented in Section 2. Experimental results, description of the used databases and performance metrics for evaluation are presented in Section 3. Detail discussion about the robustness and efficiency of the algorithm is presented in Section 4. Finally, the conclusion is drawn in Section 5.

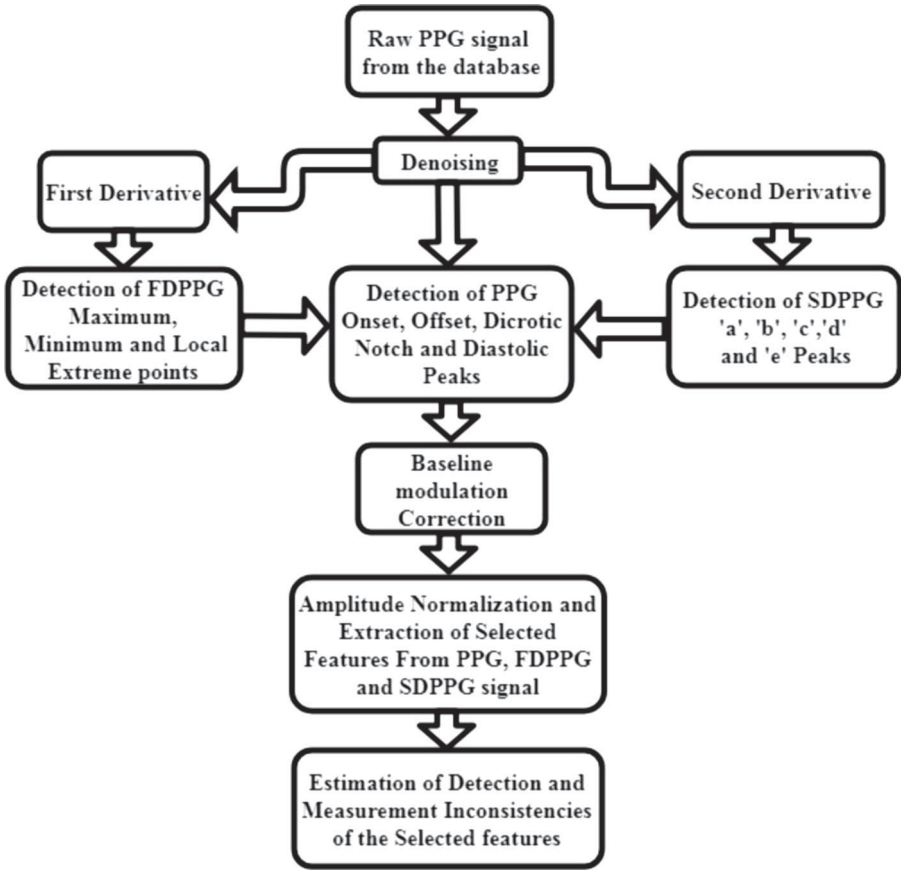

Figure 2: Block schematic of the proposed methodology. The algorithm consists of two stages: fiducial point detection (based on amplitude thresholding, slope-reversal and an empirical formula-based approach), and then feature extraction.

2. PROPOSED METHODOLOGY

The algorithm is presented in two steps: characteristic point identification using simple mathematical methods followed by features extraction and is presented in the form of a block schematic diagram in Figure 2.

2.1 Preprocessing

PPG signal amplitude is known to be influenced by the light at the photo-detector, poor blood perfusion of the peripheral tissues and different types of motion artifacts. These factors may cause signal deterioration [28] at various steps of signal acquisition and analysis. Since the adopted method is based on signal derivative, this makes the algorithm noise sensitive. Therefore, the digitally acquired PPG signals are initially denoised using a 6th order Butterworth low-pass filter with a cut-off frequency of 15 Hz, to remove any high-frequency noise components and to retain essential clinical bandwidth of the PPG signal.

2.2 Derivatives Computation

The first and second derivative of the denoised PPG signal are computed using the following equations:

$$FDPPG = \frac{d}{dt}(V_{PPG}) = \frac{d}{dt}[y(t+1) - y(t)], \tag{1}$$

$$SDPPG = \frac{d}{dt}(FDPPG) = \frac{d}{dt}[y(t+1) + y(t-1) - 2y(t)]. \tag{2}$$

Here $y(t)$ is the present sample and $y(t-1)$ and $y(t+1)$ represent the previous and the next sample respectively. Usually, the first derivative of the signal is considered as equivalent to the high pass filter. Although in reality apart from removing any low-frequency components of the signal, it also enhances the high slope regions in the signal and improves the detection accuracy of various characteristics points.

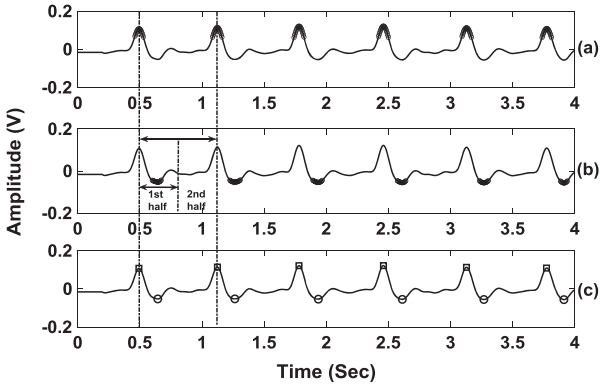

Figure 3: (a) Samples with amplitudes greater than a pre-determined threshold value are marked to identify maximum peaks; (b) FDPPG peak-to-peak interval is divided into two halves and samples in the first half of the interval between two FDPPG maximum peaks with amplitudes less than a pre-determined threshold value are marked to identify FDPPG minimum peaks; (c) detected FDPPG maximum peaks are indicated by square symbol and the FDPPG minimum peaks are indicated by circle.

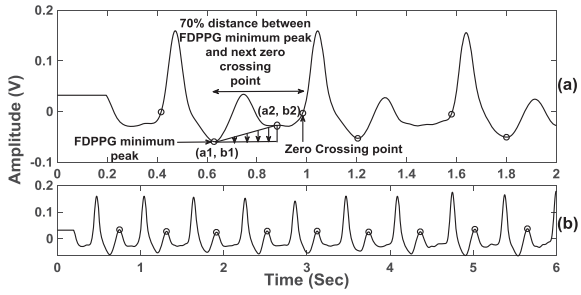

Figure 4: (a) Local extreme point detection between the FDPPG minimum peak and the next zero crossing point using an empirical formula; (b) detected local extreme points are encircled in the FDPPG signal.

2.3 Identification of FDPPG Characteristic Points

In this section, first derivative of the PPG waveform (FDPPG) is analyzed to identify FDPPG maximum peak, minimum peak and local extreme point. The methodology is described in detail as follows.

2.3.1 Detection of FDPPG Maximum Peak

Primarily based on the amplitude range, maximum amplitude of the entire FDPPG signal is calculated at first. Then FDPPG samples with amplitude greater than a fixed threshold value of 50% are marked as shown in Figure 3(a). The threshold percentage is empirically selected based on extensive tests on different types of data. This amplitude thresholding process helps to identify the higher amplitude regions on the FDPPG data. FDPPG maximum points are then identified from each of these selected regions by searching for the slope reversal points within fixed windows of 0.25 s as indicated by the square symbol in Figure 3(c).

2.3.2 Detection of FDPPG Minimum Peak

After successful detection of FDPPG maximum peak, the peak-to-peak interval is calculated and divided into two halves. FDPPG minimum peaks are usually searched in the first half portion of the interval between two consecutive FDPPG maximum peak locations as indicated in Figure 3(b). The amplitude range in the first half portion is subjected to another empirically chosen threshold value of 80% as shown in Figure 3(b). This approach not only narrows down the relevant search area but also helps to eliminate the possibility of selecting any other local minima point except the actual FDPPG minimum peak. FDPPG minimum peaks are then accurately identified from these selected regions by searching for slope reversal points within fixed windows of 0.25 s as indicated by the circle symbol in Figure 3(c).

Generally human heart rate under maximum variation can't exceed the highest value of 240 per minute [29]. This corresponds to 4 beats per second which leads to a minimum beat interval of 0.25 s. Hence, in order to determine FDPPG maximum and minimum peaks accurately without having a chance of identifying any false peak the window size is kept fixed to 0.25 s. The whole operation of maximum and minimum peak detection is summarized in Figure 3.

2.3.3 Detection of FDPPG Local Extreme Point

Next, 70% samples are chosen within a region of interest starting from the FDPPG minimum peak index up to the next zero crossing point. The percentage of samples to be taken is determined based on a trial and error method as shown in Figure 4. Finally, the index of local extreme point is identified within these boundary points using an empirical formula as described below.

In Figure 4(a), the minimum peak value is marked as (a_1, b_1) and the chosen 70% distant sample point as (a_2, b_2), where (a_1, a_2) represent the time values and (b_1, b_2) represent the corresponding voltage values. Now the amplitude of all the samples between these two points is modified by the empirical formula as stated in Equation (3).

$$\text{Modified sample} = [(\text{Original sample}) - m \times i - b_1]. \tag{3}$$

Here "m" is the slope between (a_1, b_1) and (a_2, b_2) points and $m = (b_2 - b_1/a_2 - a_1)$

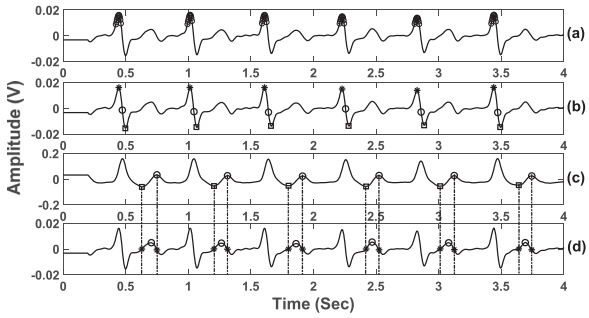

Figure 5: (a) Samples with amplitudes greater than a predetermined threshold value are marked to identify SDPPG "a" peaks; (b) detected SDPPG "a" peaks by slope reversal are indicated by star symbol, zero crossing points after "a" peaks are indicated by circle symbol and the identified "b" peaks are indicated by square symbol; (c) FDPPG minimum peaks are indicated as square symbol and the local extreme points are encircled; (d) encircled middle point indicate the location of "e" wave, between the location of minimum peak(left star) and local extreme point (right star) in the SDPPG signal.

Initially the variable "i" of Equation (3) is set to zero and then it is incremented step by step as per the sampling interval of the signal. The slope factor "m" is used to place each FDPPG sample to the same level as the starting point (a1, b1). Finally, the voltage value "b1" is subtracted to create modified FDPPG signal with a starting point of zero voltage. Now, among those modified FDPPG samples, the maximum peak location is determined at first. Then taking reference to the location of this maximum peak, a slope-reversal or slope-change point is identified in the original FDPPG signal as the location of local extreme point as shown in Figure 4.

2.4 Identification of SDPPG Characteristic Points

Next, second derivative of the PPG signal (SDPPG) waveform is analyzed to identify SDPPG "*a*" peak, "*b*" peak, "*c*" peak, "*d*" peak and "*e*" peak respectively, using the following procedures.

2.4.1 Detection of SDPPG "a" Peak

In this case also the maximum amplitude of the SDPPG data is calculated at first, based on the amplitude range of the entire SDPPG signal. Then SDPPG samples with amplitude values greater than a fixed threshold value of 45% are marked to create a proper "*a*" peak search zone as shown in Figure 5(a). The threshold value is selected entirely based on trial and error method. These selected zones are then used to identify the accurate location of "*a*" wave (star symbol) by searching for the slope reversal points as depicted in Figure 5(b) within a fixed window of 0.25 s.

2.4.2 Detection of SDPPG "b" Peak

Considering different types of SDDPG signal, sometimes limiting situation may arise in the determination of SDPPG "*b*" peak. Owing to good or poor circulation of blood in the subject, SDPPG "*b*" peak appears as global or local minima [22]. In such cases, determination of "*b*" peak as slope reversal or slope change point using amplitude threshold might appear critically challenging. In this research, after proper identification of "*a*" peak, a right traversal on the SDPPG data is carried out to determine the next zero crossing point. Then starting from the location of this zero crossing point another right traversal on the SDPPG data is carried out to determine the first SDPPG data sample with minimum slope. This point is identified as the location of "*b*" peak as shown in Figure 5(b). After extensive trial over huge database it is observed that the proposed method can efficiently deal with all the situations and come up with accurate identification of the "*b*" peaks. The whole operation of "*a*" peak and "*b*" peak detection is summarized in Figure 5(a) and (b) respectively.

2.4.3 Detection of SDPPG "e" Peak

SDPPG "e" wave location is determined in this algorithm with the help of FDPPG characteristic points. Initially, the detected FDPPG minimum point (square symbol) and the local extreme point (circle symbol) indices are mapped on the SDPPG signal as shown in Figure 5(c) and (d) respectively. Then starting from the location of FDPPG local extreme point index a left search is carried out on the SDPPG data up to the FDPPG minimum point location index till a slope reversal point is found and identified as the precise location of "*e*" wave as indicated by circle symbol in Figure 5(d).

2.4.4 Detection of SDPPG "c" Peak and "d" Peak

Accurate detection of "c" and "d" peak in the SDPPG signal is a challenging task, as the characteristics of these two small components changes rapidly with different stationary, non-stationary effects and heart rate. In the present algorithm, the region between the location of "e" and "b" peak is investigated to find the location of "c" and "d" peak. Detail methodology for the detection of "c" and "d" peak is described as follows.

Initially, starting from the location of "e" peak, a left traversal is carried out on the SDPPG data to find out the first slope reversal point as the location of "d" peak and the next slope reversal point as the location of "c" peak. This will provide information about the existence of "c" and "d" peak in the SDPPG signal. The type is illustrated

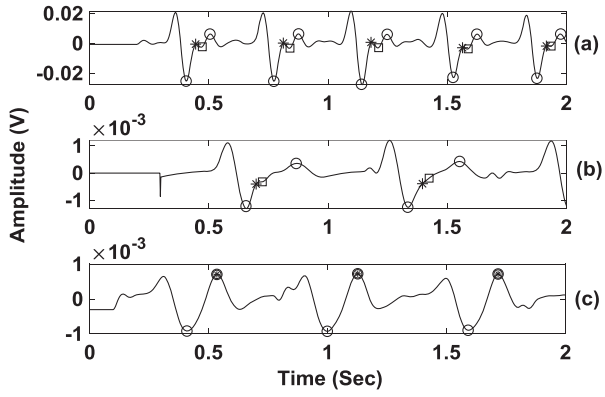

Figure 6: (a) Type-1 SDPPG signal with distinct "c" and "d" peak; (b) Type-2 SDPPG signal with distinct "c" and "d" peak (c) Type-3 SDPPG signal with merged "c" and "d" peak. Here the "c" peak is represented by star symbol and the "d" peak is represented by square symbol.

in Figure 6(a).

$$\text{Modified sample} = [(\text{Original sample}) - m \times i]. \quad (4)$$

Although, if no slope reversal point is found on the SDPPG data, then starting from the location of "b" peak, all the samples up to the location of "e" peak are modified according to an empirical formula as presented in Equation (4). The empirical formula of Equation (4) is a modified version of Equation (3). Here also the variable "i" is incremented from zero as per the sampling interval and the slope "m" is used to bring down each SDPPG sample to the level of "b" peak. Now, among those modified SDPPG samples, the maximum peak location is determined at first. Then taking reference to the location of this maximum peak, a right traversal is carried out on those modified SDPPG data sample to find out the first slope change point as the location of "c" peak and the next slope change point as the location of "d" peak. This will also provide information about the existence of "c" and "d" peak in the SDPPG signal and the type is illustrated in Figure 6(b).

However, if both of the above-mentioned logic fails, the algorithm will consider overlapping of "c", "d" and "e" peaks. This will ensure that there is no distinct "c" and "d" peak exist in the SDPPG data and the type is illustrated in Figure 6(c).

In addition, any partial detection of either "c" or "d" peak will be regarded as false detection in our present algorithm.

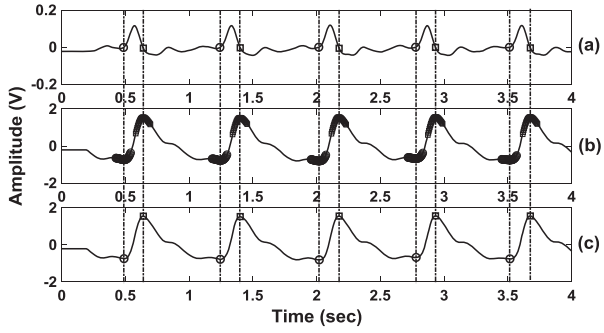

Figure 7: (a) First zero-crossing point before the primary inflection are indicated by circle-symbol and second zero-crossing point after the primary and before the secondary inflection are marked by square-symbol; (b) twenty samples are mapped on the original PPG signal taking reference to each of those zero crossing point indices (c) identified pulse onset points are indicated by circle and identified systolic peaks are marked using square symbols.

2.5 Identification of PPG Characteristic Points

Accurate identification of characteristic points from the enhanced FDPPG and SDPPG signal leads to precise identification of PPG signal characteristic points as described below.

2.5.1 Detection of Pulse Onset and Systolic Peak

Usually the zero-crossing point in a FDPPG signal before the primary inflection (Figure 1(a(ii))) is related to the pulse onset, whereas zero crossing point after the primary inflection and before the secondary inflection (Figure 1(a(ii))) is found to be related to the systolic peak of the PPG signal as shown in Figure 7(a). Considering the most recently detected FDPPG maximum peak locations as reference, left and right traversal on the FDPPG data is carried out to identify first and second zero crossing points as shown in Figure 7(a). Now twenty samples of the original PPG signal around each of such zero crossing point indices are marked to create an effective search zone as shown in Figure 7(b). Then, slope reversal or slope change point among these marked samples around the first zero crossing point is identified as the pulse onset point. Similarly, slope reversal or slope change point among those marked samples around the second zero crossing point is identified as the systolic peak as depicted in Figure 7(c).

2.5.2 Detection of Dicrotic Notch and Diastolic Peak

Generally, location and morphology of dicrotic notch and diastolic peaks are found to be highly varying under pathophysiological alteration. This imposes serious challenges for accurate identification of these two crucial points. Usually, the zero crossing points after the secondary inflection (Figure 1(a(ii))) in the FDPPG signal

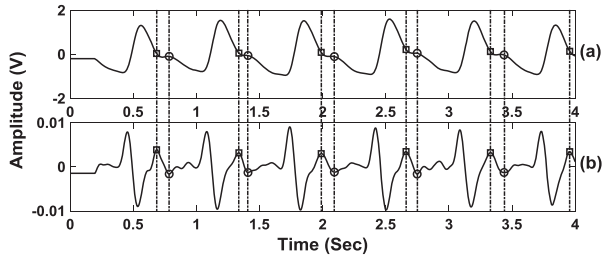

Figure 8: (a) Detected dicrotic notch points are indicated by square symbol and the diastolic peaks are encircled in the original denoised PPG signal; (b) The location of "*e*" wave in the SDPPG signal is indicated by the square symbol and the next immediate slope reversal point is encircled in the SDPPG signal.

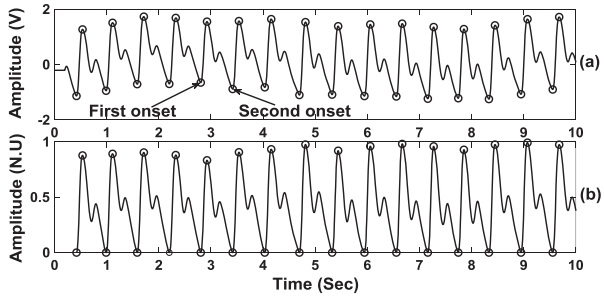

Figure 9: (a) A typical PPG record before baseline modulation correction and amplitude normalization and (b) the same PPG record after baseline modulation correction and amplitude normalization.

can be used to identify the location of dicrotic notch and diastolic peaks [20]. However, if the local extreme peak lies below the time axis, there will be no zero crossing points and in such cases, the algorithm fails. On the contrary, SDPPG wave with enhanced feature zones can always be chosen as a wise and effective alternative. In this algorithm the identified SDPPG "*e*" wave location index of Figure 8(b) is plotted to the original PPG signal to get the accurate location of the dicrotic notch or at least an incisura as depicted in Figure 8(a).

After locating SDPPG "*e*" wave successfully, a right traversal is carried out on the SDPPG data starting from the "*e*" wave location to determine the first slope reversal point as shown in Figure 8(b). This identified slope reversal point index is plotted on the original PPG signal to get the accurate location of diastolic peak as illustrated in Figure 8(a). An intense trial over a large variety of data suggests that despite of intense pathophysiological varieties; use of FDPPG minimum peak and local extreme point locations on the SDPPG data facilitates effortless, precise and easy identification of SDPPG "*e*" wave location. This, in turn, helps to identify the accurate location of dicrotic notch and diastolic peaks on the original PPG signal.

2.6 Baseline Modulation Correction and Normalization

Sometimes due to irregular breathing, body movement and as a result of unsteady finger tip contact on the sensor, baseline wander occurs in the PPG signal even within a single beat as can be seen from Figure 9(a). Since all the amplitude features are calculated with respect to a common base, any uneven signal fluctuation might lead to wrong feature values. To resolve this, the identified first pulse onset point is chosen as the baseline point of each cardiac beat as indicated in an example beat of Figure 9(a) and all the samples in between the onset points are modified according to the same empirical formula used in Equation (3). Here also the variable "i" is incremented from zero as per the sampling interval and the slope "m" is used to bring down each PPG sample to the level of the starting point (a1, b1). Finally, "b1" is subtracted to have zero voltage at the baseline points. In addition, to be able to evaluate the same feature variation among different subject, the baseline corrected PPG signal, FDPPG and SDPPG data are also subjected to amplitude normalization in the range 0–1 using Equation (5).

$$V_{\text{norm}} = \left(\frac{V_{\text{signal}} - V_{\text{signal(min)}}}{V_{\text{signal(max)}} - V_{\text{signal(min)}}} \right). \tag{5}$$

Here, V_{signal} = baseline corrected PPG/FDPPG/SDPPG signal, $V_{\text{signal(min)}}$ = minimum value of the baseline corrected PPG/FDPPG/SDPPG signal, $V_{\text{signal(max)}}$ = maximum value of the baseline corrected PPG/FDPPG/SDPPG signal. A typical PPG signal after baseline modulation correction and amplitude normalization is shown in Figure 9(b).

2.7 Feature Extraction

Accurate identification of characteristic points leads to precise extraction of different time-plane features. The proposed algorithm manages to extract more than fifty different time-plane features from PPG, FDPPG and SDPPG signals respectively, which can be used for real-time PPG based diagnostic applications as shown in Figure 10. However, for demonstration purpose only three amplitude features are selected, taken each from PPG, FDPPG and SDPPG signals. For performance comparison purpose, only six selected characteristic points is considered based on the available literatures.

The amplitude parameters reported here are measured using the formula as Amplitude = Voltage difference

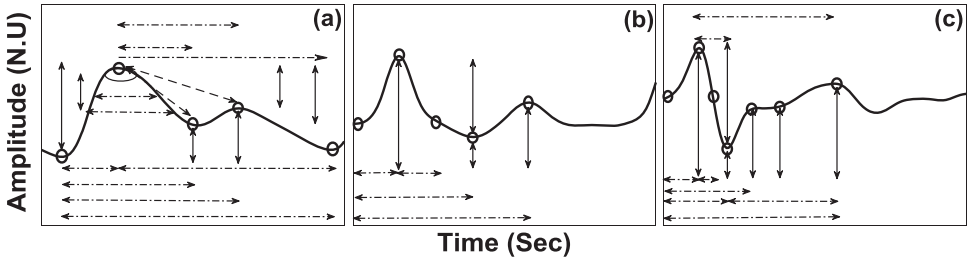

Figure 10: Detail features of (a) PPG, (b) FDPPG and (c) SDPPG signals with all detected characteristic points. Solid lines in the pictures indicate the amplitude features, dashed lines indicate the slope features, and dotdash lines indicate the duration features.

between the detected characteristic point and X-axis in normalized unit (N.U).

2.8 Detection and Measurement Inconsistency

The used databases are not annotated and so that, all the detected beats are annotated through visual inspection by the researcher and experienced medical practitioners. Furthermore, the measurement error reported in this research is not the conventional measurement error, which is usually obtained from the detected and the annotated beat. Rather in this case, visual inspection of all the records reveals that different characteristic point amplitudes and locations often deviate from cycle to cycle within the same PPG record. Similar situation is observed in the corresponding FDPPG and SDPPG records of the same PPG. Consequently, there will be some feature value inconsistency within the same record. This inconsistency is reported in the present algorithm as measurement error. The reported error can be effective to examine the amount of deviation of the same feature value within a single record. Considering total number of beats from a single record, at first, absolute difference of each feature is calculated with the earlier. Then the inconsistency is calculated out of 100 and expressed in terms of percentage. In this algorithm, the absolute amplitude measurement error and the absolute duration measurement error is computed and formulated in terms of Equations (6) and (7) respectively. However, in the present manuscript, only V_{error} is reported.

$$V_{\text{error}} = \left(\left| \frac{\sum_{i=1}^{N} V_{\text{signal}}(i) - V_{\text{signal}}(i-1)}{N-1} \right| \right) \times 100\%, \tag{6}$$

$$t_{\text{error}} = \left(\left| \frac{\sum_{i=1}^{N} t_{\text{signal}}(i) - t_{\text{signal}}(i-1)}{N-1} \right| \right) \times 100\%. \tag{7}$$

3. EXPERIMENTAL RESULTS

The developed algorithm was validated extensively over a large number of PPG records (total 23,767 PPG beats), each of one-minute duration collected from different databases. (1) The MIMIC Database (Sampling frequency 500 Hz), (2) the MIMIC II Database (Sampling frequency 125 Hz) and (3) the MIMIC Challenge Database (Sampling frequency 125 Hz), all include PPG data records from 186 ICU patients [30]. (4) Real-time PPG signal data acquired using BIOPAC MP 45 at 250 Hz sampling frequency from 90 healthy subjects and (5) also from 45 patients, admitted in the cardiology ward of Medical College and Hospital, Kolkata along with written informed consent from each subject.

The overall performance of this proposed algorithm is assessed by means of three benchmark parameters defined as follows:

$$\text{Sensitivity}(SE) = \frac{\text{TP}}{\text{TP} + \text{FN}} \times 100\%, \tag{8}$$

$$\text{Positive predictivity}(PP) = \frac{\text{TP}}{\text{TP} + \text{FP}} \times 100\%, \tag{9}$$

$$\text{Detection accuracy (Acc)} = \frac{\text{TP}}{\text{TP} + \text{FN} + \text{FP}} \times 100\%. \tag{10}$$

Here True-positive (TP) = number of accurately detected peaks, False-negative (FN) = number of peaks that are erroneously missed, False-positive (FP) = number of peaks that are erroneously detected, SE = percentage of true beats that are correctly detected by the algorithm and PP = percentage of beats detected by the algorithm that are true.

As mentioned earlier, to the best knowledge of the authors of this article, annotations of the involved databases has not been reported in anywhere and hence, for each detected beat, different statistical parameters (TP, FN, and FP) and the results are validated through visual inspection by both the researchers and trained medical practitioners of the department of cardiology,

Table 1: Overall performance of the proposed algorithm

		Systolic peak						Dicrotic notch					
Database	Total beats	TP	FN	FP	Se (%)	PP (%)	Acc (%)	TP	FN	FP	Se (%)	PP (%)	Acc (%)
MIMIC data	11,967	11,966	01	00	99.99	100	99.99	11,940	27	00	99.77	100	99.77
Normal data	7395	7395	00	00	100	100	100	7375	20	00	99.72	100	99.72
Patient data	4405	4403	02	00	99.95	100	99.95	4383	22	00	99.50	100	99.50
						Average performance							
Total	23,767	23,764	03	00	99.98	100	99.98	23,698	69	00	99.66	100	99.66
					"a" wave						"b" wave		
Database	Total beats	TP	FN	FP	Se (%)	PP (%)	Acc (%)	TP	FN	FP	Se (%)	PP (%)	Acc (%)
MIMIC data	11,967	11,961	06	00	99.95	100	99.9	11,967	00	00	100	100	100
Normal data	7395	7393	02	00	99.97	100	99.97	7393	02	00	99.97	100	99.97
Patient data	4405	4404	01	00	99.98	100	99.98	4405	00	00	100	100	100
						Average performance							
Total	23,767	23,758	09	00	99.97	100	99.97	23,765	02	00	99.99	100	99.99
					"c" wave						"d" wave		
Database	Total beats	TP	FN	FP	Se (%)	PP (%)	Acc (%)	TP	FN	FP	Se (%)	PP (%)	Acc (%)
MIMIC data	11,967	11,922	45	72	99.62	99.39	99.02	11,924	43	63	99.64	99.47	99.12
Normal data	7395	7389	06	07	99.91	99.90	99.82	7391	04	04	99.94	99.94	99.89
Patient data	4405	4359	46	37	98.95	99.15	98.13	4369	36	35	99.18	99.20	98.40
						Average performance							
Total	23,767	23,670	97	116	99.59	99.51	99.10	23,684	83	102	99.65	99.57	99.22

Table 2: Amplitudes features in normalized unit (N.U) and the corresponding percentage measurement errors

		PPG		FDPPG		SDPPG	
Database	Total beats	Avg. systolic peak amplitude (N.U)	Systolic peak amplitude (%)	Avg. max peak amplitude (N.U)	Max peak amplitude (%)	Avg. "a" wave amplitude (N.U)	"a" peak amplitude (%)
MIMIC data	11,967	0.90	3.40	0.92	2.60	0.91	2.90
Normal data	7395	0.86	3.89	0.90	2.69	0.90	3.10
Patient data	4405	0.86	4.84	0.90	3.19	0.89	4.15
				Average of all data			
Total	23,767	0.87	4.04	0.91	2.83	0.90	3.38

Medical College and Hospital, Kolkata. The overall performance of the proposed algorithm for each of the used databases is listed in Table 1. From Table 1 it can be seen that, the adopted amplitude thresholding along with windowing operation technique appears to be very promising for the detection of PPG systolic peak and SDPPG "*a*" peak efficiently with nominal failure (3 false-negative for systolic peak and 9 false-negative for "*a*" peak) due to noise, poor pulse quality or due to closer distance of the incident and the reflected wave of the PPG signal. However, 69 false-negative is reported by the algorithm to determine PPG dicrotic notch owing to critical morphological variations among different class of PPG beats and inaccurate detection of FDPPG local extreme point. Detection of "b" peak is rather straightforward, depends on successful identification of "a" peak with 2 false-negative only. However, compared to other fiducial points, detection performance of the algorithm to identify "c" and "d" peak is moderate. Because, in addition to different Stationary, non-Stationary effect, low amplitude SDPPG signals, motion artifact, irregular heart rhythm [21], erroneous detection of "b" and "e" peak and incomplete detection of "c" and "d" peak, are also responsible for the appearance of those false positive and false negative beats. The proposed algorithm exhibits significantly high Sensitivity [99.98% (systolic peak), 99.66% (dicrotic notch), 99.97% ("a" peak), 99.99% ("b" peak), 99.59% ("c" peak) and 99.65% ("d" peak)], Positive Predictivity [100% (systolic peak), 100% (dicrotic notch), 100% ("a" peak), 100% ("b" peak), 99.51% ("c" peak) and 99.57% ("d" peak)], and Detection accuracy [99.98% (systolic peak), 99.66% (dicrotic notch), 99.97% ("a" peak), 99.99% ("b" peak), 99.10% ("c" peak) and 99.22% ("d" peak)] after analyzing a total number of 23,767 PPG beats. Few Amplitude features in normalized unit (N.U) and the corresponding detection inconsistencies, extracted by the proposed algorithm are presented Table 2.

Computational processing time is an essential parameter, to assess the applicability of the proposed algorithm in hardware platform. In this research, execution time of the proposed algorithm is calculated in two separate segments: time required for characteristic point identification and the time required for feature extraction from the PPG, FDPPG and SDPPG waveforms. The algorithm

is implemented on a MATLAB platform using a personal computer having a Pentium core i3 CPU, 3.20 GHz with 4GB RAM and Windows 7 operating system. In addition, the processing times is calculated by averaging 10 execution times of the proposed algorithm on the PPG records containing 15,000 samples, taken from different databases. The time taken by the algorithm to identify all the reported characteristic points is 5.5 s (on average), whereas only 0.6 s (on average) is taken by the algorithm to extract twelve different time-plane features from a single record. As a whole, this approximate time estimation of around $(5.5 + 0.6) = 6.1$ s, taken by the algorithm suggests that it is highly eligible for hardware implementation as well as for intermittent online applications also. All the individual steps involved in the proposed algorithm have a computational complexity of

Table 3: Comparison of the proposed method with relevant studies

Ref. (Year)	Techniques used	Dataset (No. of beats)	Experimental protocol	System and processor	Se (%)	PP (%)	Acc (%)
			Systolic peak				
[17] (2015)	Hilbert transform (HT) (*high computational burden*)	Self (2,286)	In the supine position	–	100	100	100
[18] (2018)	Stationary wavelet transform (SWT) (*high computational burden*)	CSL, MIT-BIH SLP, Self (1,16,255)	Under resting condition	Intel(R), Xenon(R), CPU E5-2620 v3 at 2.4 GHz, 4 GB RAM computer	99.66	99.90	99.55
[25] (2009)	Adaptive threshold (*less computational burden*)	Self (22,623)	Both the supine position and the sitting position.	–	98.04	100	98.04
[20] (2010)	First derivative (*less computational burden*)	CSL, Fantasia, SLP (13,079, 137,830, 318,412)	–	–	99.82	99.84	99.65
					98.29	99.98	98.47
					99.19	99.99	99.18
[26] (2013)	Event-related moving average (*high computational burden*)	Self (5,071)	Sitting position	–	99.89	99.84	–
Proposed	First and second derivative (*less computational burden*)	MIMIC, Self (23,767)	Supine position	Pentium core i3 CPU, 3.20 GHz with 4 GB RAM	99.98	100	99.98
			Dicrotic notch				
[27] (1981)	Bend point (*less computational burden*)	Self (1,005)	–	–	99.90	99.80	–
[19] (1995)	First and second derivative (*less computational burden*)	Self (373)	–	HP 9000UX workstation	99.46	96.86	96.36
[20] (2010)	First derivative (*less computational burden*)	SFM database (2,564)	–	–	96.53	96.64	93.39
[23] (2016)	Second derivative (*less computational burden*)	PhysioNet (707)	–	–	99.67	99.82	–
[21] (2014)	Event-related moving average (*high computational burden*)	Self (584)	At rest on a chair	–	99.64	99.64	–
Proposed	First and second derivative (*less computational burden*)	MIMIC, Self (23,767)	Supine position	Pentium core i3 CPU, 3.20 GHz with 4 GB RAM	99.66	100	99.66
			"a" peak				
[22] (2014)	Event-related moving average (*high computational burden*)	Self (1,540)	At rest	–	99.78	100	–
[23] (2016)	Second derivative (*less computational burden*)	PhysioNet (707)	–	–	99.84	100	–
Proposed	First and second derivative (*less computational burden*)	MIMIC, Self (23,767)	Supine position	Pentium core i3 CPU, 3.20 GHz with 4 GB RAM	99.97	100	99.97
			"b" peak				
[22] (2014)	Event-related moving average (*high computational burden*)	Self (1,540)	At rest	–	99.78	99.95	
[23] (2016)	Second derivative (*less computational burden*)	PhysioNet (707)	–	–	99.84	100	
Proposed	First and second derivative (*less computational burden*)	MIMIC, Self (23,767)	Supine position	Pentium core i3 CPU, 3.20 GHz with 4 GB RAM	99.99	100	99.99
			"c" peak				
[21] (2014)	Event-related moving average (*high computational burden*)	Self (584)	At rest on a chair	–	99.82	99.82	–
Proposed	First and second derivative (*less computational burden*)	MIMIC, Self (23,767)	Supine position	Pentium core i3 CPU, 3.20 GHz with 4 GB RAM	99.59	99.51	99.10
			"d" peak				
[21] (2014)	Event-related moving average (*high computational burden*)	Self (584)	At rest on a chair	–	92.71	100	–
Proposed	First and second derivative (*less computational burden*)	MIMIC, Self (23,767)	Supine position	Pentium core i3 CPU, 3.20 GHz with 4 GB RAM	99.65	99.57	99.22

the order of "N". Since fixed numbers of steps are used, the overall computational complexity of the proposed algorithm remains of the order of "N" [$\sim$O (N)]. While implementing in MATLAB platform with core i3 processor, the time taken by the algorithm, as specified in the manuscript gives a rough idea of actual implementation. If the algorithm is implemented on a system with low processor speed, then the performance of the algorithm will be changed accordingly. However, the computational complexity will remain of the order of "N".

4. DISCUSSION

Complete identification of characteristic points from the PPG signal and its derivative under wide pathophysiological variations is a very challenging task. However, the problem is efficiently addressed in the present work in terms of a real-time automated feature extraction algorithm. From the result, it is evident that with little effort, the proposed algorithm can be applied to classify among normal and diseased PPG signals towards the development of a complete PPG based health analysis system. Advantages of the proposed algorithm are manifold as: (i) no transformation technique is used, (ii) characteristic point detection and consequent feature extraction from the PPG, FDPPG and SDPPG signals can be achieved using one comprehensive algorithm, (iii) accurate detection of some difficult to extract fiducial points such as PPG dicrotic notch, diastolic peak,SDPPG "*c*" and "*d*" wave can be efficiently addressed even in the presence of pathophysiological variations and (iv) the algorithm is found to be robust, while evaluated over a large number of normal and pathological data from different PPG databases.

The adopted derivative based approach is mathematically and computationally simple but makes the algorithm noise sensitive; hence, careful denoising is required at the preprocessing stage. Thresholding operations often need a proper readjustment for PPG signal records containing PPG beat with extremely low amplitude or PPG records containing sudden high amplitude spikes.

Although, performance of the algorithm under motion artifact corruption has not been considered in the present research, but it is acknowledged that, the presence of motion artifact will degrade the detection performance of the algorithm. However in future, during practical implementation of the proposed method, definitely we will consider some advanced filtering techniques, which will effectively remove the motion artifact corruption from the PPG signal. Moreover, it can be seen from Figure 9 that the algorithm fails to rectify the baseline-modulation of the first PPG cycle if the first sample of the PPG data belongs to any other part other than the onset point of a particular cycle. The same conclusion can also be drawn for the last cycle. Another disadvantage is that the algorithm considers partial detection of "c" and "d" peaks as false detection.

Apart from the statistical evaluations, as presented earlier, it is important to justify the efficiency and applicability of the presented algorithm by comparing it with contemporary works. In this research, the algorithms accumulated for comparison purpose are mainly based on partial characterization of the PPG signal or its derivatives due to the lack of proper literatures. However, unavailability of the coding resources from those previously reported algorithms prevents for exact reproduction of the respective algorithms. In addition, differences in used data sets, validation process, number of beats used and differences in the evaluation parameters of the mentioned literatures also present serious obstacle for exact comparison. A reasonable comparison between the proposed algorithms with the available literatures is presented in Table 3.

The comparison report as listed in Table 3 reveals that, with respect to the number of beats used, number of characteristic point extracted and pathophysiological variety, the proposed algorithm outperforms most of the reported methods and presents acceptable performance compared to the others.

5. CONCLUSION

In this research, a robust, accurate yet simple algorithm is proposed, to extract clinically relevant features from the PPG signal and its derivatives via accurate detection of characteristic points. Instead of using any computationally intensive transform technique, the proposed algorithm relies on simple derivative-based method and uses simple mathematical techniques such as amplitude threshold, slope reversal and an empirical formula based approach. This, in turn, ensures easy implementation of the algorithm in an embedded platform for portable PPG based health monitoring devices. The algorithm is extensively evaluated with a huge number of PPG signal records, collected from benchmark MIMIC databases and also from both healthy and cardiac patients. The used database also contains significant morphological and pathophysiological variations. All the extracted characteristic points are cross validated and justified through visual inspection by experienced medical practitioners. The significantly high detection accuracy as obtained for all the records proves robustness of the algorithm against wide pathophysiological variation, moderate amplitude

fluctuation and morphological diversity including sampling rate. Based on the extracted features, the algorithm can be further extended to analyze for different cardiac abnormalities. Our current work is focused on the implementation of the algorithm in an embedded platform. Through suitable interfacing with a PPG acquisition module, the device can act as a prototype PPG monitoring tool and can be used for analysis of different cardiac ailments using the extracted features.

ACKNOWLEDGEMENTS

The authors would like to express their deepest gratitude to Dr S. Guha, MD, DM (cardiology) (Professor and HOD), other medical practitioners and the entire support staffs of the department of cardiology, Medical College and Hospital, Kolkata for their valuable suggestions and assistance in the development of PPG database and validation of the proposed algorithm.

REFERENCES

1. R. Priyatharshini and S. Chitrakala, "A Self-learning fuzzy rule-based system for risk-level assessment of coronary heart disease," *IETE. J. Res.*, 1–10, Feb. 2018. https://doi.org/10.1080/03772063.2018.1431062.

2. E. T. Tan and Z. A. Halim, "Health care monitoring system and analytics based on internet of things framework," *IETE. J. Res.*, 1–8, May 2018. https://doi.org/10.1080/03772063.2018.1447402.

3. B. G. Celler and R. S. Sparks, "Home telemonitoring of vital signs – technical challenges and future directions," *IEEE. J. Biomed. Health. Inform.*, Vol. 19, no. 1, pp. 82–91, Jan. 2015.

4. B.-H. Yang, S. Rhee, and H. Asada. "A twenty-four hour tele-nursing system using a ring sensor," In *Proc. IEEE Int. Conf. Rob. Autom*, pp. 387–92, 1998.

5. J. Allen, "Photoplethysmography and its application in clinical physiological measurement," *Physiol. Meas.*, Vol. 28, no. 3, pp. R1–R39, Feb. 2007.

6. K. Reddy, B. George, N. Mohan, and V. Kumar, "A novel calibration-free method of measurement of oxygen saturation in arterial blood," *IEEE Trans. Instrum. Meas.*, Vol. 58, no. 5, pp. 1699–705, May 2009.

7. X. He, R. A. Goubran, and X. P. Liu, "Secondary peak detection of PPG signal for continuous cuffless arterial blood pressure measurement," *IEEE Trans. Instrum. Meas.*, Vol. 63, no. 6, pp. 1431–9, Jun. 2014.

8. M. T. Islam, I. Zabir, S. T. Ahamed, M. T. Yasar, C. Shahnaz, and S. A. Fattah, "A time-frequency domain approach of heart rate estimation from photoplethysmographic (PPG) signal," *Biomed. Signal. Process. Control.*, Vol. 36, pp. 146–54, Jul. 2017.

9. K. H. Chon, S. Dash, and K. Ju, "Estimation of respiratory rate from photoplethysmogram data using time-frequency spectral estimation," *IEEE Trans. Biomed. Eng.*, Vol. 56, no. 8, pp. 2054–63, Aug. 2009.

10. A. Goshvarpour and A. Goshvarpour, "Poincaré's section analysis for PPG-based automatic emotion recognition," *Chaos Solitons Fractals*, Vol. 114, pp. 400–7, Sep. 2018.

11. A. Romem, A. Romem, D. Koldobskiy, and S. M. Scharf, "Diagnosis of obstructive sleep apnea using pulse oximeter derived photoplethysmographic signals," *J. Clin. Sleep Med.*, Vol. 10, no. 8, pp. 285–90, 2014.

12. N. Mahri, K. B. Gan, R. Meswari, M. H. Jaafar, and M. A. Mohd. Ali, "Utilization of second derivative photoplethysmographic features for myocardial infarction classification," *J. Med. Eng. Technol.*, Vol. 41, no. 4, pp. 298–308, May 2017.

13. A. Sološenko, A. Petrėnas, V. Marozas, and L. Sörnmo, "Modeling of the photoplethysmogram during atrial fibrillation," *Comput. Biol. Med.*, Vol. 81, pp. 130–8, Feb. 2017.

14. A. Sološenko, A. Petrėnas, and V. Marozas, "Photoplethysmography-based method for automatic detection of premature ventricular contractions," *IEEE Trans. Biomed. Circuits Syst.*, Vol. 9, no. 5, pp. 662–9, Oct. 2015.

15. A. Reisner, P. A. Shaltis, D. McCombie, and H. H. Asada, "Utility of the photoplethysmogram in circulatory monitoring," *Anesthesiology*, Vol. 108, no. 5, pp. 950–8, May 2008.

16. M. Elgendi, "On the analysis of fingertip photoplethysmogram signals," *Curr. Cardiol. Rev.*, Vol. 8, no. 1, pp. 14–25, Jan. 2012.

17. B. R. Ferro, A. R. Aguilera, and R. r. Fernández De La Vara Prieto, "Automated detection of the onset and systolic peak in the pulse wave using Hilbert transform," *Biomed. Signal. Process. Control.*, Vol. 20, pp. 78–84, Jul. 2015.

18. S. Vadrevu and M. S. Manikandan, "A robust pulse onset and peak detection method for automated PPG signal analysis system," *IEEE Trans. Instrum. Meas.*, Vol. 68, no. 3, pp. 807–17, Mar. 2019.

19. M. J. Oppenheim and D. F. Sittig, "An innovative dicrotic notch detection algorithm which combines rule-based logic with digital signal processing techniques," *Comput. Biomed. Res.*, Vol. 28, no. 2, pp. 154–70, Apr. 1995.

20. B. N. Li, M. C. Dong, and M. I. Vai, "On an automatic delineator for arterial blood pressure waveforms," *Biomed. Signal. Process. Control.*, Vol. 5, no. 1, pp. 76–81, Jan. 2010.

21. M. Elgendi, "Detection of c, d, and e waves in the acceleration photoplethysmogram," *Comput. Methods Programs Biomed.*, Vol. 117, no. 2, pp. 125–36, Nov. 2014.

22. M. Elgendi, I. Norton, M. Brearley, D. Abbott, and D. Schuurmans, "Detection of a and b waves in the acceleration photoplethysmogram," *Biomed. Eng. Online*, Vol. 13, no. 1, pp. 139(1–18), Sep. 2014. https://doi.org/10.1186/1475-925X-13-139.

23. M. Soundararajan, S. Arunagiri, and S. Alagala, "An adaptive delineator for photoplethysmography waveforms," *Biomed. Eng./Biomedizinische Technik*, Vol. 61, no. 6, pp. 645–55, Jan. 2016.

24. D. G. Jang, S. H. Park, and M. Hahn, "Framework for automatic delineation of second derivative of photoplethysmogram: A knowledge-based approach," *J. Med. Biol. Eng.*, Vol. 34, no. 6, pp. 547–53, Jan. 2014.

25. H. S. Shin, C. Lee, and M. Lee, "Adaptive threshold method for the peak detection of photoplethysmographic waveform," *Comput. Biol. Med.*, Vol. 39, no. 12, pp. 1145–52, Dec. 2009.

26. M. Elgendi, I. Norton, M. Brearley, D. Abbott, and D. Schuurmans, "Systolic peak detection in acceleration photoplethysmograms measured from emergency responders in tropical conditions," *PLoS ONE*, Vol. 8, no. 10, e76585 (pp. 1–11), Oct. 2013.

27. P. Kinias, H. Fozzard, and M. Norusis, "A real-time pressure algorithm," *Comput. Biol. Med.*, Vol. 11, no. 4, pp. 211–20, Jun. 1981.

28. J. A. Sukor, S. J. Redmond, and N. H. Lovell, "Signal quality measures for pulse oximetry through waveform morphology analysis," *Physiol. Meas.*, Vol. 32, no. 3, pp. 369–84, Mar. 2011.

29. S. K. Mukhopadhyay, M. Mitra, and S. Mitra, "ECG feature extraction using differentiation, Hilbert transform, variable threshold and slope reversal approach," *J. Med. Eng. Technol.*, Vol. 36, no. 7, pp. 372–86, May 2012.

30. A. L. Goldberger, L. A. N. Amaral, L. Glass, J. M. Hausdorff, P. C. Ivanov, R. G. Mark, J. E. Mietus, G. B. Moody, C.-K. Peng, and H. E. Stanley, "Physiobank, PhysioToolkit, and PhysioNet," *Circulation*, Vol. 101, no. 23, pp. e215–e220, 2000.

Authors

Abhishek Chakraborty received his B.Sc. (Hons.) and M.Sc. degrees in electronic science from the University of Calcutta, Kolkata, India in 2005 and 2007 respectively. Currently, he is pursuing his Ph.D. degree in the Department of Applied Physics, University of Calcutta, India. He is also working as a part-time Lecturer (Government approved) in the Department of Electronics, Dum Dum Motijheel College, Kolkata since 2009. He qualified the UGC –NET examination in the year 2013. His research interests include biomedical signal processing and analysis.

Email: acaphy_rs@caluniv.ac.in

Deboleena Sadhukhan received her B.Sc. degree with major in Physics in 2007. She then completed her B. Tech and M. Tech degrees in Instrumentation Engineering from the Department of Applied Physics, University of Calcutta, India, in 2010 and 2012 respectively, and stood 1st class first (gold medalist) in both of them. She is currently pursuing her Ph. D. degree from the same department with the prestigious DST INSPIRE fellowship provided by the Department of Science & Technology, Government of India. Her research interests include biomedical signal processing and pattern recognition.

Email: dsaphy_rs@caluniv.ac.in

Madhuchhanda Mitra was born in Kolkata, India in 1961. She received her B.Tech, M.Tech. and Ph.D (Tech) degrees in 1987, 1989 and 1998, respectively, from University of Calcutta, Kolkata, India. She is currently a Professor with the Department of Applied Physics, University of Calcutta. Her current research interests include biomedical signal processing, machine fault analyses, and material science. Dr. Mitra received the "Griffith Memorial Award" from the University of Calcutta.

Corresponding author. Email: mmaphy@caluniv.ac.in